Copyright WILEY-VCH Verlag GmbH & Co. KGaA, 69469 Weinheim, Germany, 2014.

ADVANCED MATERIALS

Supporting Information

for *Adv. Mater.,* DOI: 10.1002/adma.201306091

An Ultrathin, Smooth, and Low-Loss Al-Doped Ag Film and Its Application as a Transparent Electrode in Organic Photovoltaics

*Cheng Zhang, Dewei Zhao, Deen Gu, Hyunsoo Kim, Tao Ling, Yi-Kuei Ryan Wu, and L. Jay Guo**

Supporting Information

Ultra-thin, Smooth, and Low-loss Al-doped Ag Film as Transparent Electrode with Application in Organic Photovoltaics

Cheng Zhang, [†] *Dewei Zhao,* [†] *Deen Gu, Hyunsoo Kim, Tao Ling, Yi-Kuei Ryan Wu, and L. Jay Guo**

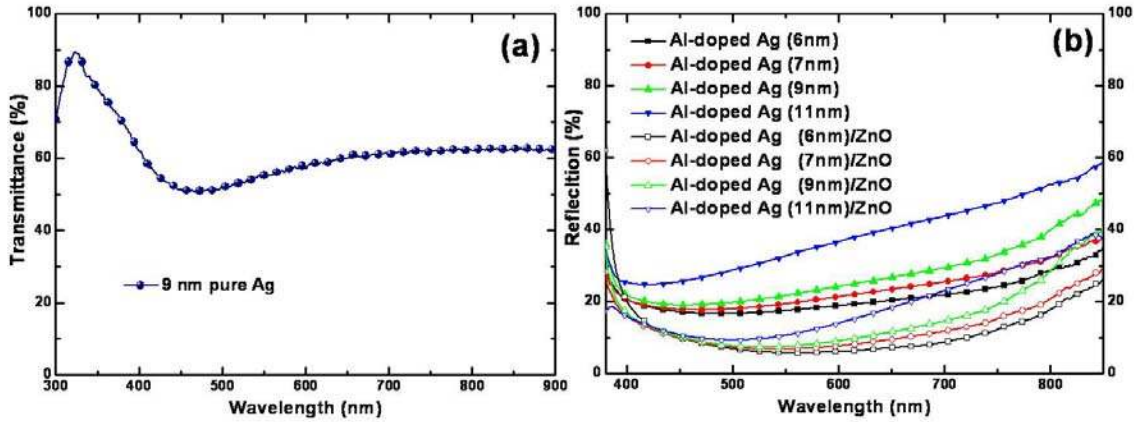

Figure S1. (a) Transmittance spectrum of 9 nm pure Ag film. (b) Reflection spectra of Al-doped Ag films and Al-doped Ag/ZnO films with different thickness (6, 7, 9, and 11 nm).

For transmission measurement, the spectrum from a bare fused silica substrate was taken as the reference. For reflection, the spectrum was normalized to that from a thick (opaque) Ag mirror. It is true that a thick Ag film absorbed a small amount of incident light and the reflection is not 100%, but this method could give reasonable results.

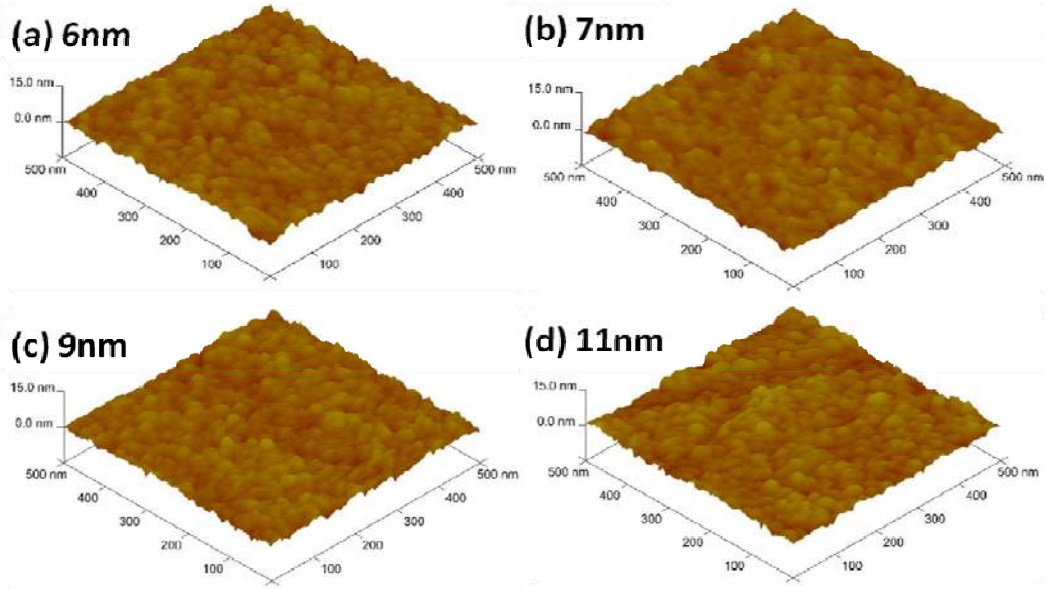

Figure S2. 3D Tapping-mode AFM images of Al-doped Ag films (a) 6 nm, (b) 7 nm, (c) 9 nm, and (d) 11 nm, showing the RMS roughness of 0.815 nm, 0.782 nm, 0.859 nm, and 1.00 nm, respectively. All films are deposited on fused silica substrates. The scan size is 500 nm × 500 nm.

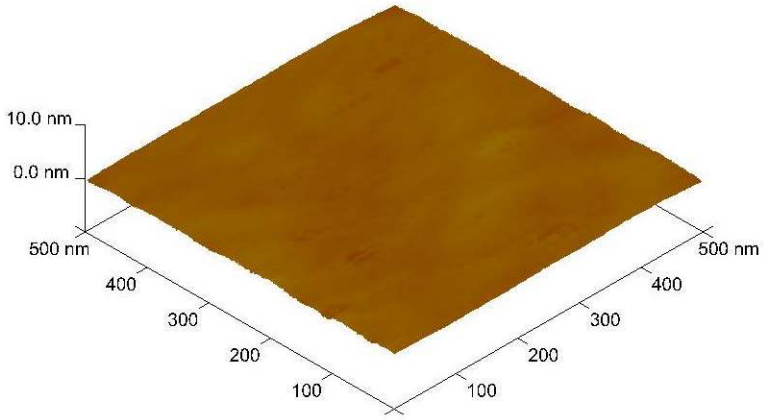

Figure S3. 3D Tapping-mode AFM image of bare fused silica substrate. The scan size is 500 nm × 500 nm. The RMS roughness is 0.195 nm and R_{max} is 1.81 nm. The result indicates that fused silica surface is pretty smooth; therefore, the effect of substrate surface roughness on film roughness is negligible.

Detailed AFM images of Al-doped Ag films with different thickness are shown in Figure S2, with RMS roughness less than 1 nm. In order to exclude the influence of the surface profile of the fused silica substrate, we first measured its surface topography, which has a fairly smooth feature with an RMS roughness around 0.2 nm (Figure S3). Therefore, its influence on film roughness can be neglected.

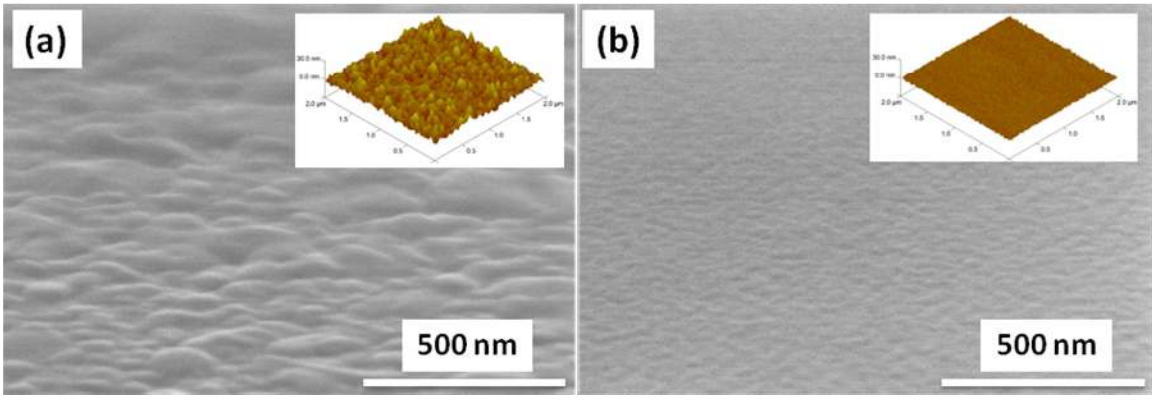

Figure S4. SEM images of (a) 100 nm pure Ag film and (b) 100 nm Al-doped Ag film. The insets in each figure are their corresponding tapping mode AFM images. All films are deposited on fused silica substrates. The scale bar for AFM images in (c) and (d) is 30 nm. The scale bar for SEM images is 500 nm. The 100 nm pure Ag film has an RMS roughness of 3.38 nm and R_{max} of 28.3 nm, 3 times as those of 100 nm Al-doped Ag film (1.10 nm and 9.95 nm).

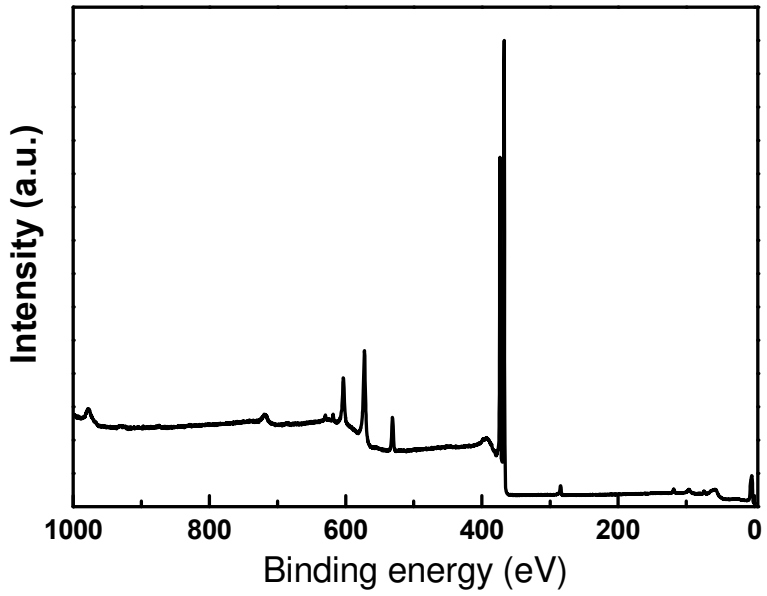

Figure S5. XPS spectrum for the "300 W Ag and 200 W Al" combination recorded by survey scanning. The atomic concentration of Al was determined from the peak areas of Al2p and Ag3d by their respective atomic sensitivity factors.

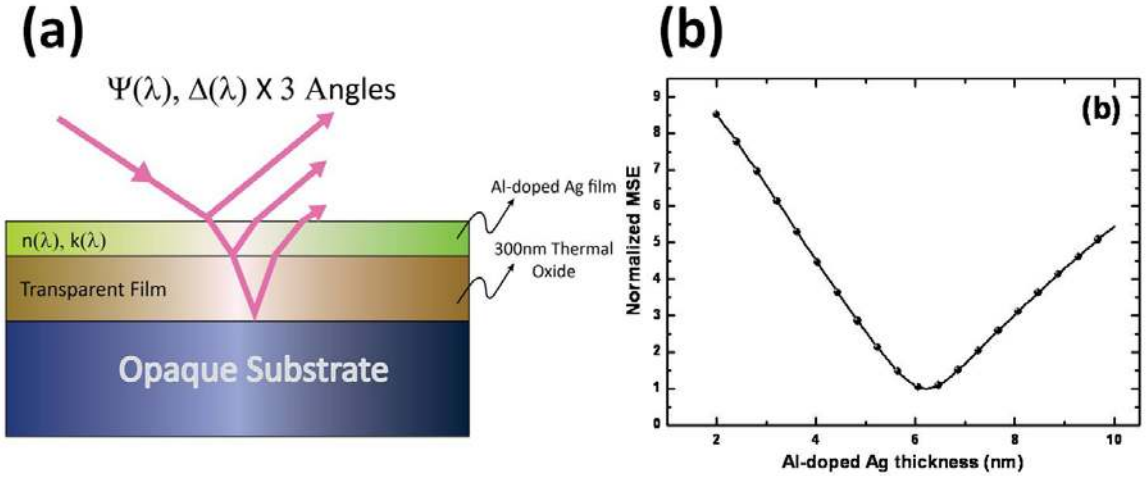

Figure S6. (a) Schematic of ellipsometry measurement procedure for interference enhancement method. (b) Thickness fitting uniqueness of 6 nm Al-doped Ag film.

In ellipsometer measurement, Ψ(λ) and Δ(λ) are measured at three different angles. They are related to the intensity and phase change of the S and P polarized light after reflection upon the sample. Afterwards, Ψ(λ) and Δ(λ) are used to fit the optical constants (n and k) and the thickness d of the film. In a thin absorbing film case, the fitting is not unique, as the change of reflection intensity can come from either the absorption coefficient of the film or the film thickness. To break up this correlation, a thin transparent layer (SiO_2 in our measurement) is

put beneath the absorbing film. It provides extra reflected light and thus additional information for later data fitting. Using this "interference enhancement" method, both the film optical constants and thickness can be uniquely determined. Figure S4b shows the normalized fitting error with Al-doped Ag thickness for the 6 nm case. There is minimum/converging fitting error at 6 nm, a direct evidence of the ultra-thin feature of our Al-doped Ag film. Therefore, we were able to experimentally confirm that the 6 nm film thickness which is consistent with the nominal thickness based on our deposition rate calibration.

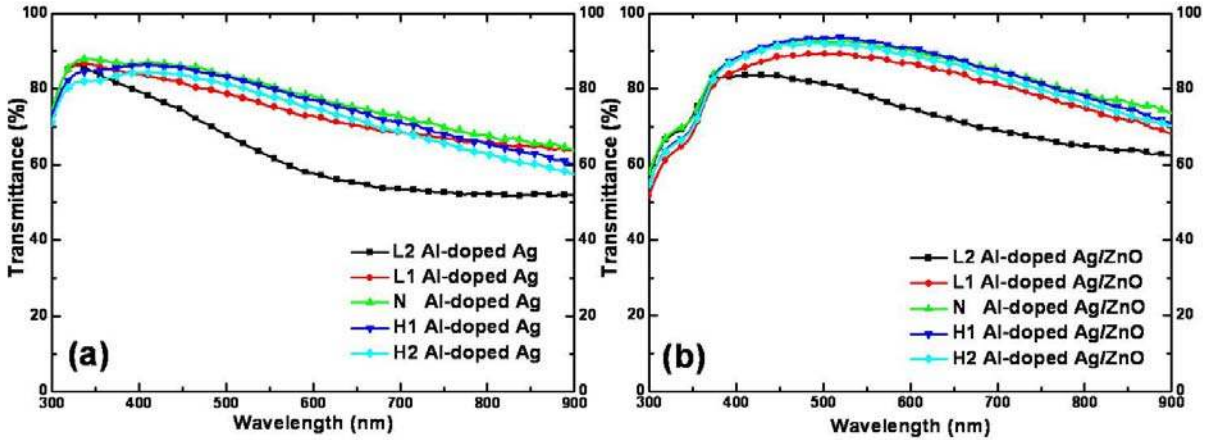

Figure S7. Transmittance spectra of (a) 7 nm Al-doped Ag films and (b) 7 nm Al-doped Ag/ZnO films with different Al doping concentrations.

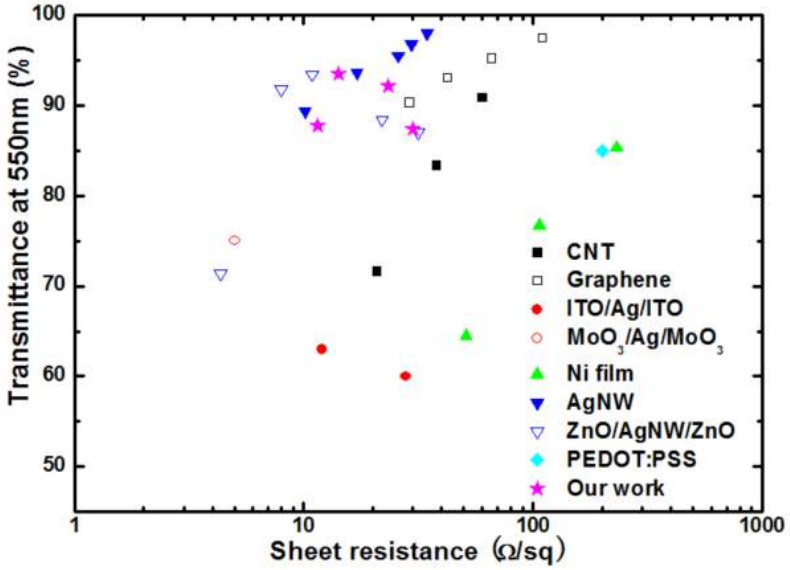

Figure S8. Comparison of optical transmittance (at 550 nm) versus sheet resistance for our work Al-doped Ag/ZnO and other reported works: CNT (ref.1), Graphene (ref.2), ITO/Ag/ITO (ref.3), MoO_3/Ag/MoO_3 (ref.4), nickel thin films (ref.5), silver nanowires (AgNW) (ref.6), ZnO/AgNW/ZnO (ref.7), PEDOT:PSS (ref.8). Note that all selected data are based on their applications in optoelectronic devices.

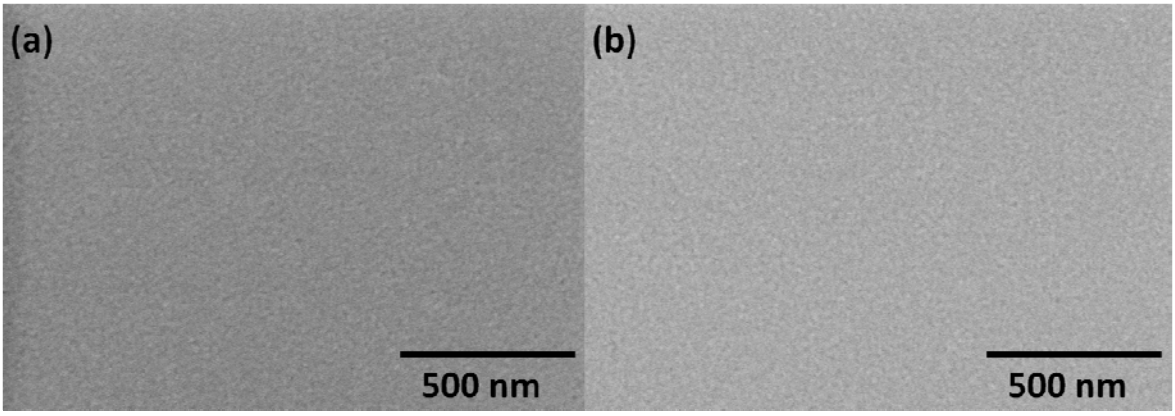

Figure S9. SEM images of 9 nm Al-doped Ag films (a) before and (b) after annealing treatment (at 150 ^{o}C in N_2 environment for 15 min).

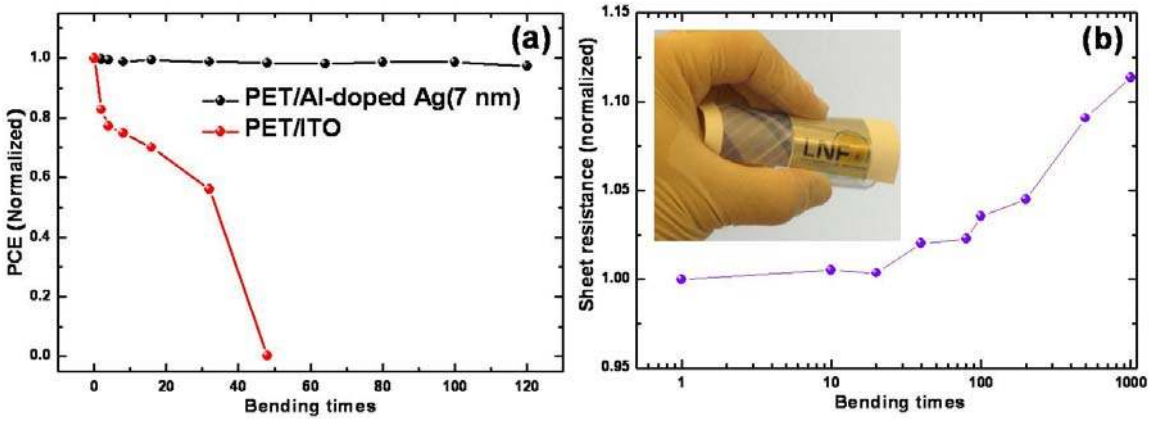

Figure S10. (a) Bendability test of the devices with PET/ITO and PET/Al-doped Ag as electrodes with bending times. (b) Sheet resistance of Al-doped Ag film versus bending times. The inset shows a photo of Al-doped Ag film on PET substrate.

The ultra-thin film deposited on flexible PET film shows excellent mechanical stability as compared with ITO on PET. The ITO based device significantly degraded each time it was bent, and stopped operating altogether after being bent 40 times (Figure S10a). On the contrary, the 7 nm Al-doped Ag based device has much more stable performance even after 120 bending cycles, showing no obvious performance degradation. The film sheet resistance increased by only 10% after being bent 1000 times (Figure S10b).

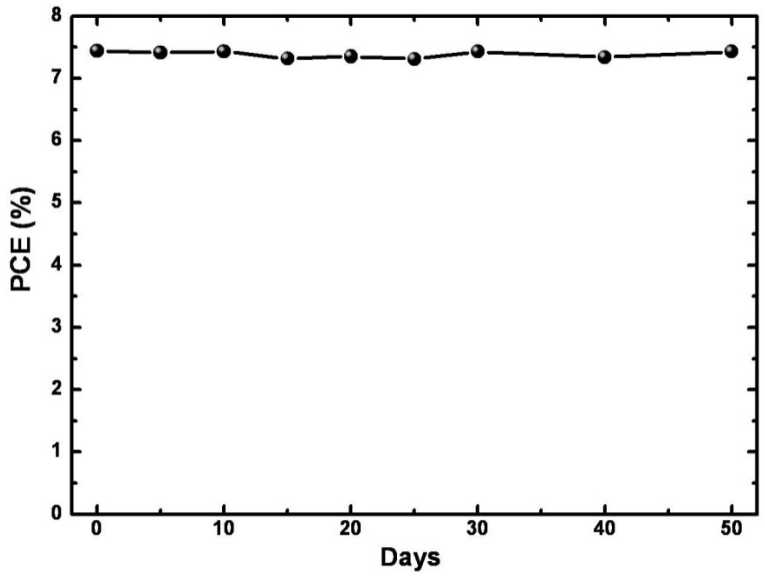

Figure S11. Dependence of the PCE of the device with Al-doped Ag film as electrode on the storage time.

The robustness of Al-doped Ag film over time is another unique and important feature. The sputtered films were kept in atmosphere without protection layers, and no obvious change in color and transparency was observed even after more than 1 month. Long-term stability of the electrode is crucial in practical applications in organic electronics. Figure S11 shows the dependence of the PCEs of the Al-doped Ag based devices on the storage time. The result indicates that the device with Al-doped Ag film as electrode has stable performance over time.

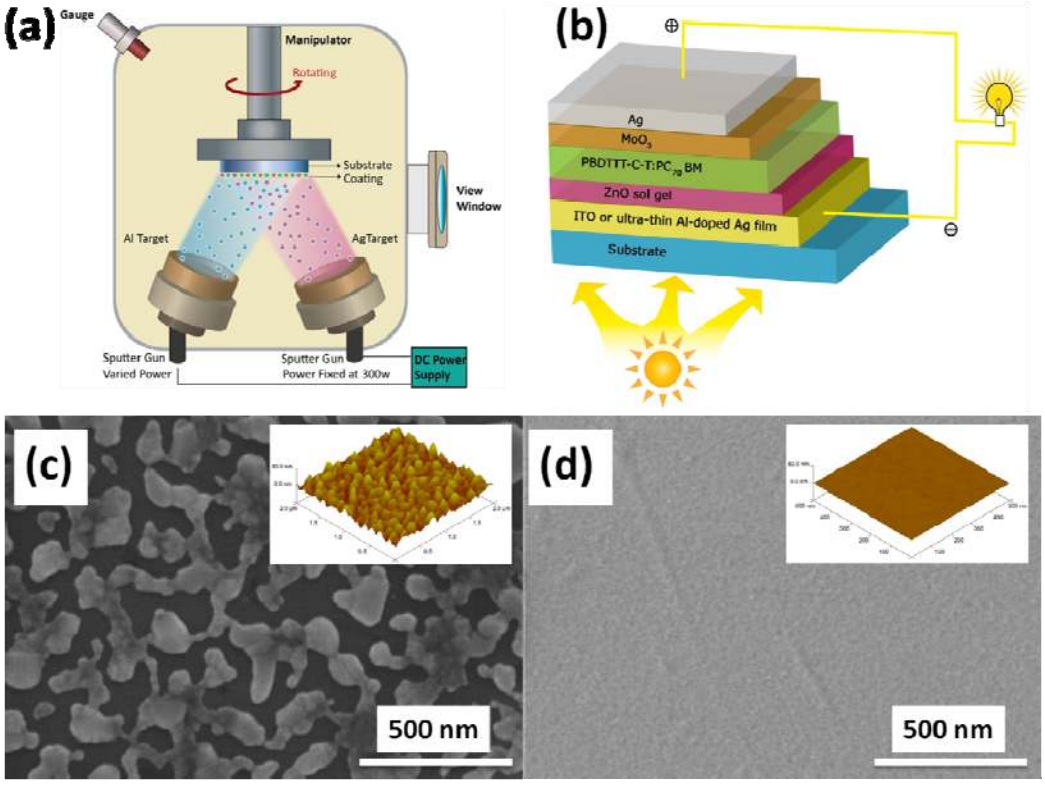

Figure S12. (a) Set-up of co-deposition of Ag and Al. (b) Schematic of the OPV devices with ITO or ultra-thin Al-doped Ag film as electrodes. SEM images of (c) 9 nm pure Ag film, (d) 9 nm Al-doped Ag film. The insets in (c) and (d) are their corresponding AFM images. All

films are deposited on fused silica substrates. The 9 nm pure Ag film has an RMS roughness of 10.8 nm, 12 times higher than 9 nm Al-doped Ag film (0.86 nm).

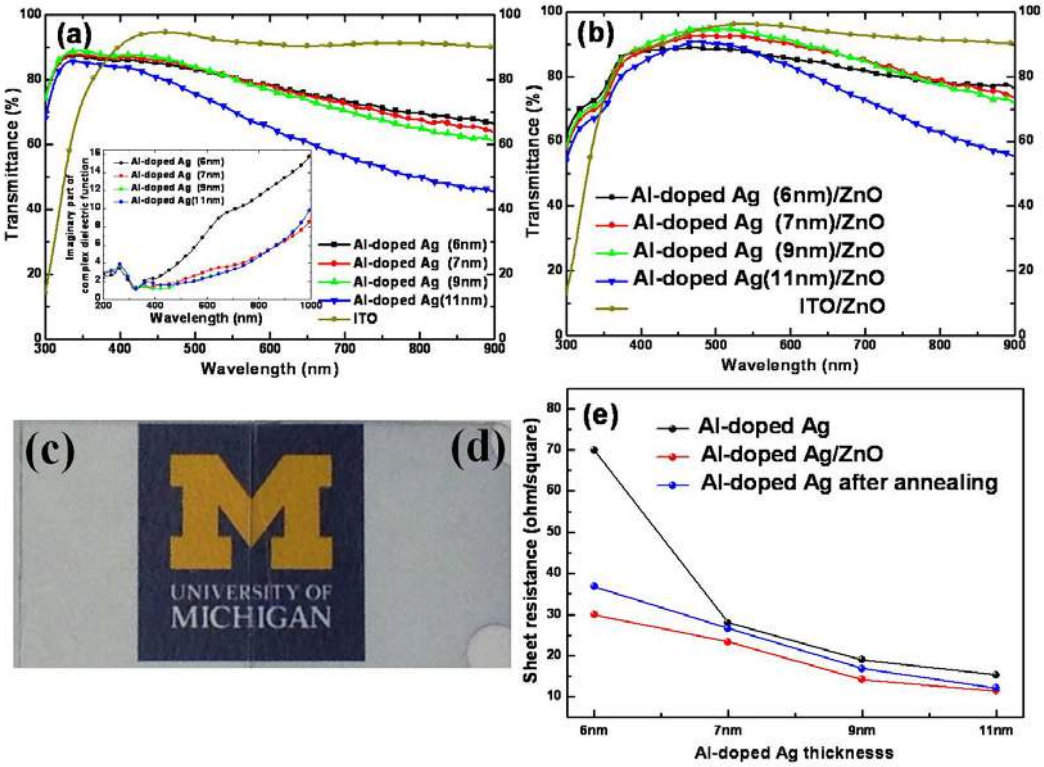

Figure S13. Transmittance spectra of (a) Al-doped Ag films and (b) Al-doped Ag/ZnO films with different thickness (6, 7, 9, and 11 nm), in which ITO and ITO/ZnO films are shown as well. Photos of (c) ITO/ZnO and (d) 7 nm Al-doped Ag/ZnO transparent conductors in front of a colored logo. The inset of in (a) compares the dependence of the imaginary part of the complex dielectric function on the wavelength for Al-doped Ag films with different thickness (6, 7, 9, and 11 nm). (e) Sheet resistance versus Al-doped Ag film thickness (black: Al-doped Ag film; red: Al-doped Ag/ZnO film; blue: Al-doped Ag film after annealing in N_2 environment).

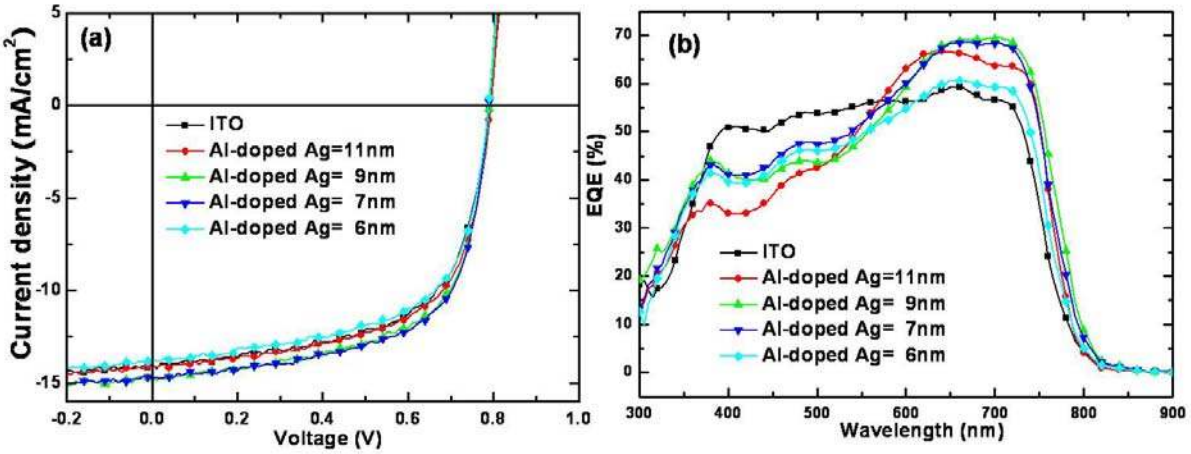

Figure S14. (a) *J-V* characteristics of ITO based and ultra-thin Al-doped Ag based OPVs. (b) EQEs of ITO based and ultra-thin Al-doped Ag based OPVs.

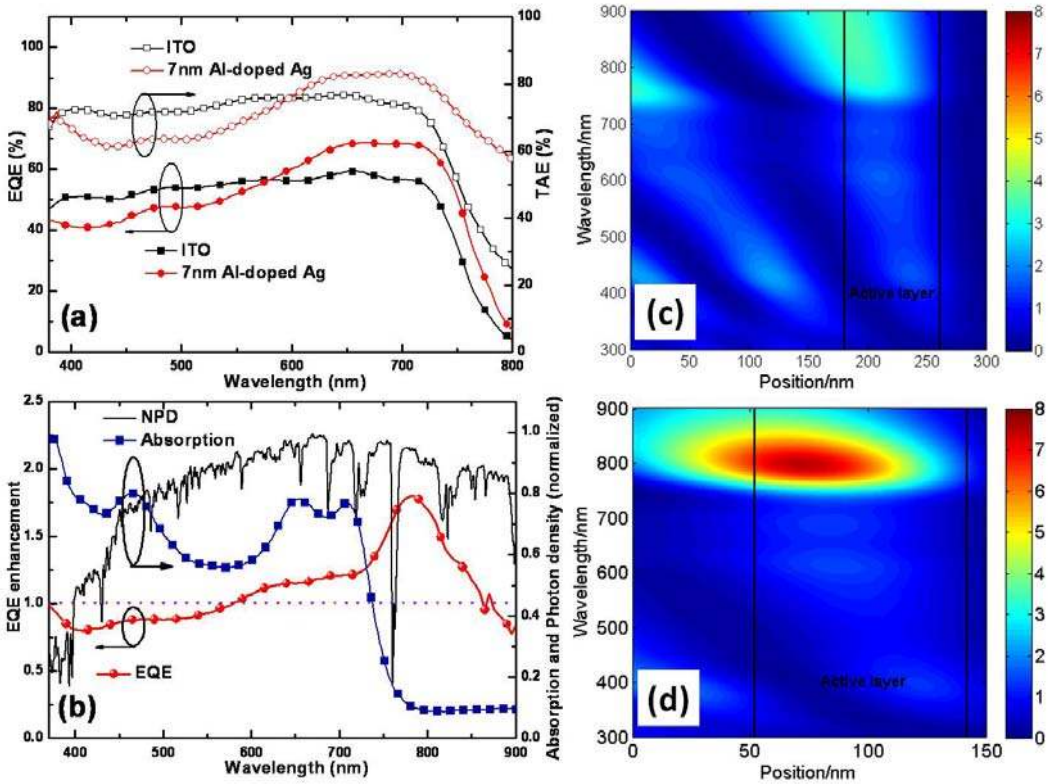

Figure S15. (a) TAEs and EQEs of ITO and 7 nm Al-doped Ag based devices. (b) EQE and TAE enhancements of 7 nm Al-doped Ag based device over ITO based device, as well as the normalized absorption spectrum of PBDTTT-C-T:$PC_{70}BM$ active layer and normalized photon density of AM1.5G solar light. Simulation of the optical field intensity ($|E|^2$) distribution versus position and wavelength in (c) ITO based device and (d) 7 nm Al-doped Ag based device, where the enhanced optical field in the active layer around 800 nm is responsible for the measured EQE enhancement at the same wavelength range shown in Fig. 5b.

Table S1. Summary of the main photovoltaic parameters of the devices with ITO and Al-doped Ag films with different thickness as electrode.

	Transmittance @ 550 nm (%)		Sheet resistance (Ω/sq)	
Al-doped Ag	Before ZnO	After ZnO	Before ZnO	After ZnO
L2	62.2	78.3	28.3	22.3
L1	75.4	88.2	27.0	21.6
N	81.0	92.2	28.0	23.4
H1	80.2	92.5	28.5	23.9
H2	78.0	90.9	29.2	24.1

Table S2. Summary of the main photovoltaic parameters of the devices with ITO and Al-doped Ag films with different thickness as electrode.

	J_{SC} [mA cm^{-2}]	V_{oc} [V]	FF [%]	PCE [%]	R_s [Ω·cm^2]	R_{sh} [Ω·cm^2]
ITO	14.00	0.80	61.3	6.87	4.0	462.9
Al-doped Ag=11nm	14.03	0.80	62.0	6.95	3.9	460.0
Al-doped Ag= 9nm	14.70	0.80	62.5	7.35	3.3	498.2
Al-doped Ag= 7nm	14.76	0.80	63.0	7.44	3.0	512.5
Al-doped Ag= 6nm	13.71	0.80	61.3	6.72	3.4	368.0

An ITO-based device has a PCE of 6.87%, with a short-circuit current density (J_{sc}) = 14.00 mA cm^{-2}, open-circuit voltage (V_{oc}) = 0.80 V, and fill factor (FF) = 61.3%. Devices built using Al-doped Ag films of various thicknesses as transparent cathodes produce consistently better efficiency than those made produced with ITO electrodes. Note that the device made with 6 nm Al-doped Ag has similar performance to ITO-based devices. To our knowledge, this investigation demonstrates the thinnest Ag film produced without any wetting layer, especially when used as electrodes in OPVs [ref.9]. With the decrease of film thickness from 11 nm to 7 nm, J_{sc} and FF increase, producing a maximum PCE of 7.44% at 7 nm. However, further decrease of Al-doped Ag thickness to 6 nm lowers the J_{sc} and decreases PCE to 6.72%. The identical measured V_{oc}'s of 0.8 V imply that favorable Ohmic contacts are formed at both anode and cathode electrodes for either ITO or Al-doped Ag film by the use of interfacial metal oxide layers, MoO_3 and ZnO. Therefore the V_{oc} is essentially determined by the difference between the highest occupied molecular orbital (HOMO) of poly[4,8-bis-(2-ethylhexyloxy)-benzo[1,2b:4,5b0]dithiophene-2,6-diyl-alt-4-(2-ethylhexyloxy)-thieno-[3,4b]thiophene-2,6-diyl] (PBDTTT-C-T) (Solarmer) and the lowest unoccupied molecular orbital (LUMO) of [6,6]-phenyl C71-butyric acid methyl ester ($PC_{70}BM$) (American Dye Sources Inc.). Meanwhile, the FFs of ITO and Al-doped Ag based devices are comparable, due to the good contacts of ITO or Al-doped Ag with a ZnO layer, resulting in similar series resistances as shown in Table S2. Therefore, it can be concluded that the increase in the PCE of the Al-doped Ag based devices primarily originates from the enhancement of J_{sc}

Experimental Section

Film deposition: The Al-doped Ag films were co-sputtered on fused silica substrates by a DC magnetron sputter tool (Kurt J. Lesker Co. Lab18) with Argon gas at room temperature (Figure 1a). The chamber base pressure was pumped down to about 1×10^{-6} Torr before sputtering. In the deposition, the Argon gas pressure was 4.5 mTorr and the substrate holder was rotated at 10 rpm. Two pure Ag and Al targets were co-sputtered to create the ultra-thin Al-doped Ag film. By varying target source power, the composition of the film was controlled. In this experiment, the Ag target power was fixed at 300 W, while the Al target power was adjusted to 100, 150, 200, 300, and 400 W. Varying Al power would change the Al-doped Ag film composition accordingly. The calibrated Ag deposition rate at 300 W was 0.9 nm s^{-1} and Al deposition rate at 200 W was 0.06 nm s^{-1}. These slow deposition rates allow accurate control of the film thickness. Films with different compositions were prepared and studied.

Film characterization: The thicknesses of Al-doped Ag films were calculated based on the calibrated deposition rate, being subsequently confirmed by spectroscopic ellipsometry measurement (J. A. Woollam M-2000). The sheet resistance was measured by Miller FPP-5000 4-Point Probe. The absorption, reflection, and transmittance spectra were recorded using UV-VIS-NIR spectrometer. Scanning electron microscopy (SEM) (Hitachi SU8000) and tapping mode atomic force microscopy (AFM) (Veeco NanoMan) were used to characterize the surface topography of films on fused silica substrate. X-ray photoelectron spectroscopy

(XPS) (Kratos Axis Ultra XPS) was employed to determine the Al-doped Ag film composition.

Device fabrication: Control devices were fabricated on ITO coated glass substrates with a sheet resistance of 12 Ω sq^{-1}. The substrates were cleaned in an ultrasonic bath with acetone and isopropyl alcohol for 10 min. After sputtering, the ultra-thin Al-doped Ag films and ITO substrate were transferred into a glove box filled with N_2 for ZnO coating. ZnO sol gel solution was prepared as reported [ref. 10] and was spin-coated on top of ITO and Al-doped Ag films, followed by baking at 70 ^oC for 5 min. Then ZnO sol gel coated substrates were taken out of glove box and baked at 150 ^oC for 15 min in air, forming a 45 nm ZnO layer. After baking, the substrates were transferred into the glove box again for polymer active layer deposition. A blend solution made of PBDTTT-C-T and $PC_{70}BM$ with a weight ratio of 1:1.5 in chlorobenzene (25 mg mL^{-1}) with 3 vol% 1,8-diiodooctane (DIO, Sigma-Aldrich) was spin-coated onto ITO and Al-doped Ag substrates to form an active layer (90 nm). Subsequently, MoO_3 (6 nm) and Ag (100 nm) were evaporated sequentially (1×10^{-6} mbar) (Kurt J. Lesker). The final cells have an isolated electrode with a diameter of 1 mm. The device architecture is shown in Figureb. The inverted devices in this study have a structure of ITO or ultra-thin Al-doped Ag/ZnO/PBDTTT-C-T:$PC_{70}BM$/MoO_3/Ag.

Device characterization: The current density-voltage (*J-V*) characteristics were measured using a Keithley 2400 system while illuminating the solar cells with AM 1.5 G simulated sunlight generated by an Oriel Solar Simulator at an irradiation intensity of 100 mW/cm^2. The incident power intensity at one sun (100 mW cm^{-2}) was calibrated using a Si reference cell. The devices were measured in the atmosphere without any encapsulation. The EQE measurement was performed in a nitrogen glove box and EQE spectra were obtained using light from a 200 Hz-chopped and monochromated Xenon-lamp, calibrated against a silicon solar cell.

References

[1] D. S. Hecht, L. Hu, G. Irvin, Adv. Mater. **2011**, 23, 1482.
[2] S. Bae, H. Kim, Y. Lee, X. Xu, J.-S. Park, Y. Zheng, J. Balakrishnan, T. Lei, H. Ri Kim, Y. I. Song, Y.-J. Kim, K. S. Kim, B. Ozyilmaz, J.-H. Ahn, B. H. Hong, S. Iijima, Nat Nano **2010**, 5, 574.
[3] J. Yun, W. Wang, T. S. Bae, Y. H. Park, Y.-C. Kang, D.-H. Kim, S. Lee, G.-H. Lee, M. Song, J.-W. Kang, ACS Appl. Mater. & Interfaces **2013**, 5, 9933.
[4] H. Jin, C. Tao, M. Velusamy, M. Aljada, Y. Zhang, M. Hambsch, P. L. Burn, P. Meredith, Adv. Mater. **2012**, 24, 2572.
[5] D. S. Ghosh, L. Martinez, S. Giurgola, P. Vergani, V. Pruneri, Opt. Lett. **2009**, 34, 325.
[6] D.-S. Leem, A. Edwards, M. Faist, J. Nelson, D. D. C. Bradley, J. C. de Mello, Adv. Mater. **2011**, 23, 4371.
[7] A. Kim, Y. Won, K. Woo, C. H. Kim, J. Moon, ACS Nano **2013**, 7, 1081.
[8] D. Gupta, M. M. Wienk, R. A. J. Janssen, Adv. Energy Mater. **2013**, 3, 782.
[9] N. P. Sergeant, A. Hadipour, B. Niesen, D. Cheyns, P. Heremans, P. Peumans, B. P. Rand, Adv. Mater. **2012**, 24, 728.
[10] A. K. K. Kyaw, X. W. Sun, C. Y. Jiang, G. Q. Lo, D. W. Zhao, D. L. Kwong, Appl. Phys. Lett. **2008**, 93, 221107.